communications biology

A Nature Portfolio journal

Article

https://doi.org/10.1038/s42003-025-08989-7

An uncharacterized small protein MicN mediates the transcriptional reprogramming of *Salmonella* through regulating the RpoS-RNA polymerase interaction

Check for updates

Ruirui Liu[1,2,7], Qi Wang[1,3,7], Xilu Yuan[1,2,7], Yingying Yue[1,2], Ping Zhang[1,2], Kun Yin[3], Weiwei Wang[1,2,4] ✉ & Bingqing Li[1,2,4,5,6] ✉

Salmonella adapts its metabolism upon entry into macrophages to survive in the hostile host environment. However, the specific regulatory mechanisms involved remain largely unknown. In this study, we identify a previously uncharacterized small protein, MicN, that is essential for the survival of *Salmonella* within macrophages and significantly influences its pathogenicity in vivo. The expression of MicN induces substantial alterations in the metabolic pathways of *Salmonella*, notably resulting in promoting a transition to a low-energy metabolic state. We determined the crystal structure of MicN, revealing the protein conformation characterized by a high density of negatively charged regions on its surface. Employing a pull-down assay, we established that MicN primarily interacts with RNA polymerase (RNAP). Computational modeling of the interaction between MicN and RNA polymerase subunits suggested a strong likelihood of binding between MicN and RpoS. Further validation through both in vivo and in vitro experiments confirmed the direct interaction of MicN and RpoS. The predicted MicN-RpoS structure indicated that the binding of MicN to RpoS modifies RpoS's interaction with RNAP core enzyme, and functional assays confirmed that MicN indeed changes the binding affinity of RpoS to RNA polymerase. This research provides the first insight into how *Salmonella* utilizes specific small proteins to finely tune transcriptional reprogramming, thereby establishing a foundational understanding of the intracellular survival mechanisms of pathogens and paving the way for the development of novel therapeutic strategies.

Salmonella enterica subtype Typhimurium (*S. Typhimurium*), an important gram-negative intracellular vacuolar bacterium, has emerged as a significant public health menace[1]. Particularly, with the escalating prevalence of antibiotic-resistant strains, the treatment and prevention of *Salmonella*-related diseases have been greatly complicated and challenging. *Salmonella* can establish infection within macrophages, where these infected macrophages act like a "Trojan horse" facilitating the spread of *Salmonella* to various tissues, thereby initiating a systemic infection[2,3]. Macrophages serve as a critical colonization niche for *Salmonella* survival, replication, and dissemination after infection, despite a harsh environment within characterized by an acidic pH ranging from 4.5 to 5.5, and the presence of antimicrobial peptides, oxygen, and nitrogen-free radicals[4–8]. To adapt to

[1]Department of Clinical Laboratory, Shandong Provincial Hospital Affiliated to Shandong First Medical University, Jinan, Shandong, China. [2]Department of Pathogen Biology, School of Clinical and Basic Medical Sciences, Shandong First Medical University & Shandong Academy of Medical Sciences, Jinan, Shandong, China. [3]Shandong Institute of Parasitic Diseases, Shandong First Medical University & Shandong Academy of Medical Sciences, Jining, Shandong, China. [4]Hospital for Skin Diseases, Shandong First Medical University, Jinan, Shandong, China. [5]School of Pharmaceutical Sciences, Medical Science and Technology Innovation Center, Shandong First Medical University & Shandong Academy of Medical Sciences, Jinan, Shandong, China. [6]Key Lab for Biotech-Drugs of National Health Commission, Jinan, Shandong, China. [7]These authors contributed equally: Ruirui Liu, Qi Wang, Xilu Yuan.
✉e-mail: wangweiwei_fly@126.com; bingqingsdu@163.com

this intracellular niche, *Salmonella* has evolved a series of survival strategies, with the most important being the active regulation of cellular metabolism processes. The temporal and conditional regulation of transcription initiation is the most economical means and effectively achieve a trade-off between activities devoted to reproduction and those devoted to stress-resistant repair[9].

One major strategy employed by *Salmonella* to modify transcriptional reprogram of their genome and adapt to environmental changes is through the interactions of RNA polymerase (RNAP) core enzyme ($\alpha_2\beta\beta'\omega$) with various types of alternative σ factors, forming the holoenzyme Eσ that binds to different types of promoters to coordinate and direct the transcription initiation of specific subsets of genes in response to environmental perturbations[10]. Among these σ factors, RpoS (also called σ38 or σS) serves as the master regulator that protects many Gram-negative bacteria from detrimental environmental conditions, allowing bacteria to maintain survival in various stresses, including extreme low pH, high temperatures, nutrient deprivation, oxidative damage, and osmotic pressure[11–13]. Global transcriptomic analyses revealed that RpoS controls the expression of up to 20% genes in *Escherichia coli*, with these genes involved in stress protection, alternative metabolic pathways, membrane biosynthesis, cell motility, and pathogenicity[14–17]. Additionally, it also plays an indispensable roles in virulence, biofilm formation, and antibiotic tolerance in a variety of human pathogens such as *S. Typhimurium*, *E. coli*, and *Pseudomonas aeruginosa*[18–20]. The involvement of RpoS in the formation and maintenance of persister cells has also been confirmed in several bacterial species[21,22]. It is evident that by controlling the expression and activity of RpoS, it is possible to achieve rapid global transcriptional pattern adjustments to counteract the adverse effects of environmental perturbations.

Intracellular levels of RpoS are rapidly, tightly, and exquisitely regulated by cells to maintain a dynamic equilibrium of its production and activity[23]. This complex regulation involves multiple pathways of positive and negative control at the transcriptional, translational, and post-translational levels, ensuring that RpoS expression and activity are restricted under inappropriate conditions[12]. Currently, Crl is the only known regulator that specifically enhances RpoS activity through direct interaction, increasing RpoS's affinity for core RNAP and thus stimulating the expression of RpoS-dependent genes[24–26]. Additionally, the modulation of the free conformation of RpoS may also serve as a mechanism to regulate its stability and activity. An illustration of this is the ATP-dependent degradation of RpoS by the ClpXP protease complex, where the binding of RssB to RpoS and the resulting conformational change are essential for its delivery to ClpXP[12]. In contrast, a common strategy for controlling other σ factor activity involves their sequestration by anti-sigma factors, which prevent σ factors from binding to RNAP[10,27]. For example, Rsd specifically sequesters σ70 and can actively remove it from the σ^{70}-RNAP complex[28–30]. Moreover, anti-σ^I factors contribute to the heat stress response and virulence in *Clostridia* and *Bacilli*, and dual membrane-spanning anti-sigma factors (Dma) that control outer membrane vesicle biogenesis have been identified in *Bacteroides thetaiotaomicron*[31,32]. It is noteworthy that no anti-sigma factors for RpoS have been reported to date.

In this study, we identified and characterized a small protein, MicN (GenBank ID: WP_000657897.1), which plays a critical role in the pathogenicity of *Salmonella*. Through analysis of the crystal structure of MicN and subsequent in vitro validation, we demonstrated that MicN directly interacts with the stress-induced transcription factor RpoS. This interaction reduces the expression of RpoS-regulated genes, leading *Salmonella* to adopt a low-energy metabolic strategy. Under conditions such as macrophage infection and carbon starvation, *Salmonella* rapidly increases the expression level of MicN, which subsequently silences aerobic respiration and promotes the utilization of ethanolamine. This reprogramming, mediated by MicN, enhances the survival of *Salmonella* within macrophages and under antibiotic stress. Thus, MicN serves as an effective strategy for the bacterium to adapt to the stressors present within host cells. In summary, we identified MicN as an anti-sigma factor of RpoS that plays a crucial role in modulating bacterial metabolism. We also elucidated its mechanisms and significance in enhancing stress tolerance and facilitating the infection of host cells by *S. Typhimurium*.

Results

MicN plays a crucial role in the pathogenicity of *Salmonella*

The investigation of the interplay between genes and pathogenicity remains a pivotal focus within pathogen research. We identified MicN (STM14_RS14310), a previously uncharacterized protein in *S. Typhimurium* ATCC 14028S, which exhibits significant upregulation during macrophage infection. Notably, we observed a variety of compelling phenotypes associated with this protein. The *micN* gene is located within the Gifsy-1 pathogenicity island of the *Salmonella* chromosome and spans 189 nucleotides (nt) (Fig. 1a)[33]. The tRNA-Arg gene is located upstream of *micN*, while downstream lies *gogA*, which encodes a type III effector protease. In fact, the open reading frame (ORF) of *micN* is embedded within the sRNA (*isrI*), and it was only recently confirmed through experimental studies that it can encode a small protein[34,35]. Therefore, the functions of the MicN protein remain largely unexplored. The genomic landscape surrounding MicN is enriched with phage-related genes, suggesting a potential historical occurrence of horizontal gene transfer. Evidence indicates that MicN contributes to adaptations under environmental stress, and previous studies have demonstrated its marked upregulation in response to desiccation, carbon starvation, and the invasion of epithelial cells[36–38]. Moreover, we have observed a similar upregulation of MicN during *Salmonella* infection in macrophages, consistent with previous findings[37] (Fig. 1b). Although the expression levels of MicN have been previously examined, its precise function remains to be elucidated.

To elucidate the function of MicN, we generated a full-frame knockout mutant Δ*micN* (deficient in the *micN* gene, derived from the *S. Typhimurium* ATCC 14028S background), which exhibited growth curves similar to those of the wild type (Fig. S1). We then investigated the potential effects of MicN on the intracellular survival of *Salmonella* within macrophages. RAW264.7 cells, which serve as a robust in vitro model for murine macrophages, were infected with either *S. Typhimurium* ATCC 14028S (wild type) or the Δ*micN* mutant at a multiplicity of infection (MOI) of 10 for 2 h. Samples were collected at 2 h intervals to evaluate the intracellular replication of *Salmonella*. Our results demonstrated that the intracellular replication of the wild-type strain significantly exceeded that of the Δ*micN* mutant throughout the sampling period (Fig. 1c), suggesting that MicN plays a crucial role in enhancing the intracellular adaptation of *Salmonella*.

After ingestion, *Salmonella* initially invades intestinal epithelial cells and is actively phagocytosed by macrophage after the traversal of the epithelial barrier. To further explore the impact of MicN on *Salmonella* invasion, we conducted phenotypic assays using HT-29 cells to determine its influence on invasive capacity. Notably, the invasion efficiency of the Δ*micN* mutant was markedly elevated compared to the wild-type strain, showing an increase of 55.69% after infection (Fig. 1d). These findings suggest that MicN may influence the expression of SPI-1-related genes, a hypothesis supported by subsequent investigations. But there is no difference shown in the release of lactate dehydrogenase (LDH), which serves as a marker for cell death or damage (Fig. 1e). Actually, the enhanced invasion rate caused by the absence of *micN* could pose a disaster for host survival. To evaluate the survival of infected hosts, C57BL/6 mice were intraperitoneally injected with either the wild-type or Δ*micN* strains, and their survival times were monitored (Fig. 1f). The result revealed that mice infected with the Δ*micN* strain exhibited significantly shortened survival times compared to the control group ($p = 0.0016$) (Fig. 1g). This aligns with the invasion experiments, indicating that MicN may serve a regulatory role in maintaining optimal invasion efficiency of *Salmonella*, thereby enabling the pathogen to sustain access to resources for prolonged survival within the host. Collectively, these results underscore the critical function of MicN in modulating intracellular survival and invasion capacity.

MicN significantly influences the formation of persisters

Despite lacking antibiotic resistance genes, some clinical pathogens can withstand antibiotic treatment by entering a persister state[39]. This

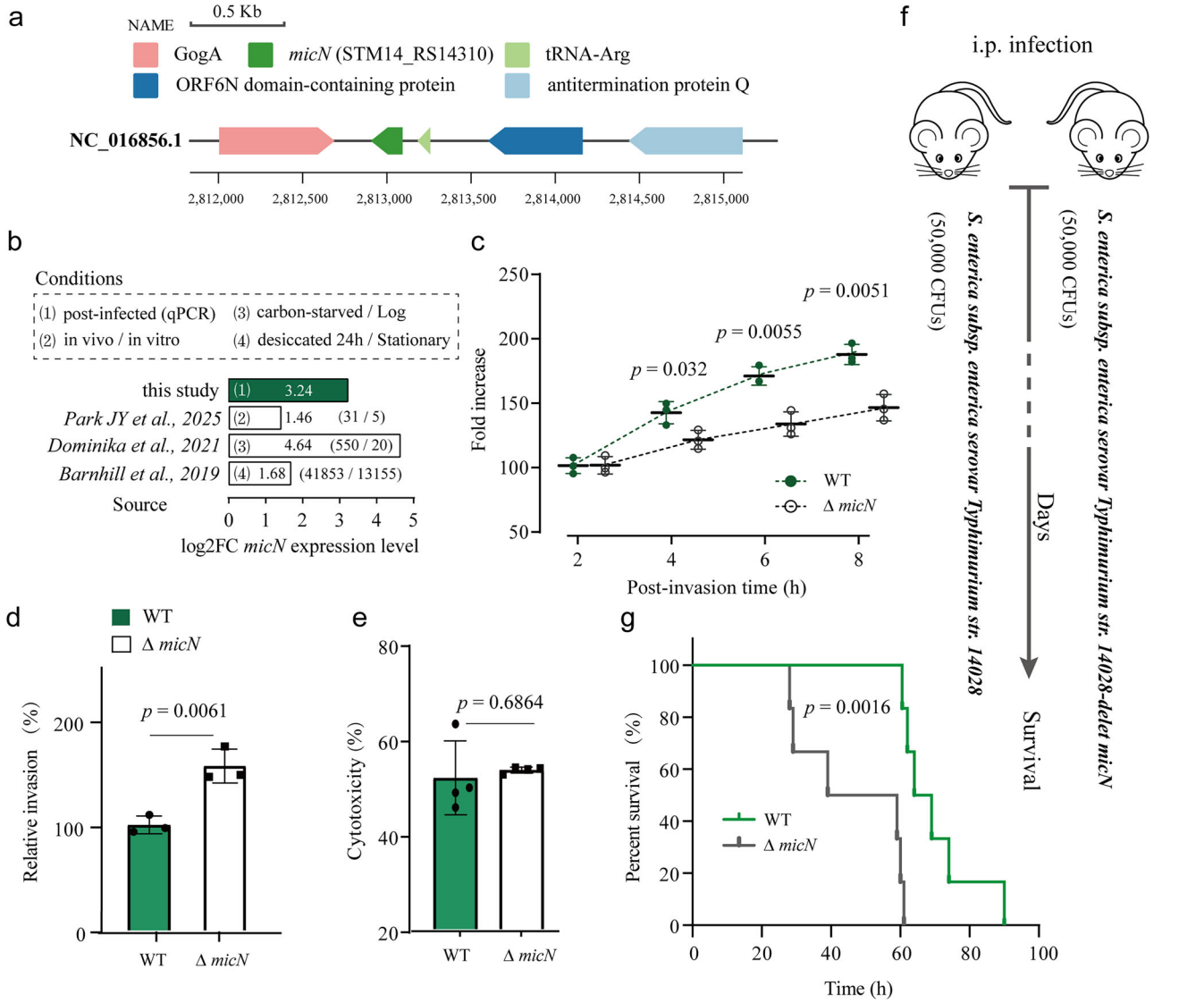

Fig. 1 | MicN is intricately linked to the intracellular survival and pathogenicity of *Salmonella*. **a** The genomic landscape of *micN*. **b** Conditions under which *Salmonella* up-regulates *micN* expression are illustrated. The TPM values are indicated in parentheses. **c** Comparison of intracellular survival capabilities between wild-type and Δ*micN* strains within RAW264.7 macrophages. **d** Assessment of invasion capabilities of wild-type and Δ*micN* strains in HT-29 cells. **e** Measurement of cytotoxicity, indicated by lactate dehydrogenase (LDH) release. **f** Schematic representation of the infection survival test. **g** Survival curves of C57BL/6 mice following infection with equal quantities of wild-type and Δ*micN* strains, with survival monitored every 3 h. Error bars indicate STDEV, and data are derived from at least three independent experiments.

strategy is often achieved by bacterial stress responses or diminished energy metabolism. Interestingly, the phenotypic effects associated with MicN appear to be consistent with those observed in persister. To investigate the role of MicN in antibiotic stress responses and persister formation, we performed antibiotic tolerance experiments on Δ*micN*/wild-type using multiple antibiotics with different mechanisms of action. Ampicillin inhibits the synthesis of peptidoglycan in the cell wall, colistin disrupts membrane integrity, and gentamicin interferes with ribosomal function during protein synthesis[40].

We initially performed in vitro experiments to further investigate the survival curves of wild-type and Δ*micN* in the presence of gentamicin, ampicillin, and colistin. The wild-type strain exhibited markedly higher survival rates and demonstrated greater resistance to the ribosome 30S subunit inhibitors (gentamicin) and the cell membrane targeting antibiotic (colistin) (Fig. 2a, b). The initial survival curves for gentamicin displayed distinct biphasic kinetics, indicating that the survival ratio after the inflection point was primarily attributable to persisters. While the bacterial killing curve under colistin treatment did not clearly indicate biphasic characteristics, the proportion of surviving wild-type bacteria between 2 and 24 h was significantly higher than that of the Δ*micN* mutant. This difference may be attributed to the potent bactericidal effect of colistin, which targets the cell membrane and leads to the death of all tested strains. It is worth noting that, no significant difference was observed between wild-type and Δ*micN* strains following exposure to ampicillin in the in vitro assays. We hypothesize that the absence of a peptidoglycan layer may not lead to rapid lethality in *Salmonella*, as cell lysis necessitates the synergy of osmotic pressure. We subsequently assessed the intracellular survival curves of the Δ*micN* mutant compared to the wild-type strain under ampicillin treatment. Either Δ*micN* or wild-type was introduced into RAW264.7 macrophages at an MOI of 10 for 1 h, followed by exposure to ampicillin. Samples were collected at 0 ~ 8 h post-infection, and intracellular levels of *Salmonella* were quantified using CFU counting method. The in vivo infection models revealed a reduced intracellular survival of the Δ*micN* strain compared to the wild-type strain following ampicillin treatment (Fig. 2c), underscoring the critical role of MicN.

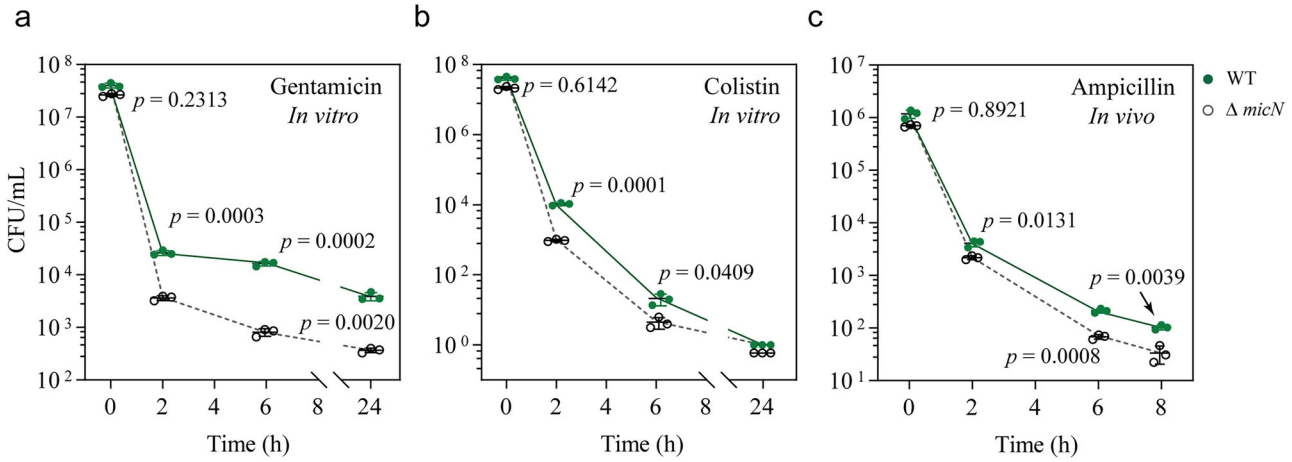

Fig. 2 | MicN contributes to persister formation in *Salmonella*. **a**, **b** CFU of *Salmonella* wild-type and Δ*micN* after exposure to 50 ug/mL of gentamicin (**a**) and 40 μg/mL of colistin (**b**), respectively. **c** Colony-forming units (CFU) of *Salmonella* wild-type and Δ*micN* following treatment with ampicillin 20 μg/mL in RAW264.7 macrophages. Error bars indicate STDEV, and data are derived from at least three independent experiments.

In summary, the presence of MicN significantly enhances the survival of *Salmonella* under antibiotic pressure and could lead to an increased intracellular load within macrophages, aligning with our prior findings. Additionally, wild-type strains exhibited consistently higher survival rates compared to the Δ*micN* mutant from 2 to 8 h post-infection, underscoring a significant role of MicN in the long-term intracellular viability of *Salmonella* and suggesting it may be part of a key component of a survival strategy employed by various pathogens.

Transcriptomic analysis of *Salmonella* following MicN expression

To further elucidate the biological functions associated with MicN, a pBAD24-*micN* vector designed for robust expression of *micN* was constructed and subsequently introduced into the Δ*micN* strain (denoted as p*micN*). As a control, the original arabinose-induced plasmid pBAD24 was introduced into the Δ*micN* strain. The obtained strains were induced to express the gene using 0.05% arabinose. Subsequently, we assessed the gene transcriptomes between p*micN* and Δ*micN* strains under identical conditions. A total of 297 genes exhibited over 2-fold up-regulation upon overexpression of *micN*, while 266 genes were down-regulated. To gain a broad overview of the p*micN* transcriptional landscape, we performed enrichment analyses on the Gene Ontology (GO) and Kyoto Encyclopedia of Genes and Genomes (KEGG) annotations of the DEG gene sets. A total of 442 GO terms were annotated for the differentially expressed genes, with 90 terms being significantly enriched ($p < 0.05$) (Fig. 3a). We found that the majority of the enriched pathways had a z-score < 0, indicating that the differentially expressed genes in these pathways are primarily down-regulated. This suggests that MicN may play a role as a repressor in the regulation of gene expression in *Salmonella*. In order to gain a clearer understanding of the details, we selected the top 10 Biological Process terms for presentation and analysis (Fig. 3b). Among them, amino acid activation (GO:0043038), tRNA-aminoacylation (GO:0043039), and ribosomal protein synthesis (GO:0006418), were significantly enriched, indicating that protein synthesis in *Salmonella* is suppressed. GO:0055114 represents oxidation-reduction process, where the differentially expressed genes associated with this term predominantly focus on substrate oxidative phosphorylation and electron transport within the respiratory chain. The network relationships involved in child terms relating to electron transport were illustrated (Fig. 3c), suggesting that the major energy supply mode for aerobic respiration in *Salmonella* are inhibited. In addition, GO:0019752 relates to the carboxylic acid metabolic process, which encompasses various organic acids involved in the TCA cycle and is coupled with the electron transport chain. In summary, the differentially expressed genes indicate involvement in processes related to protein synthesis, aerobic respiration, and energy production, with a predominant downregulation of these genes. This suggests that MicN significantly impacts the basal metabolism of *Salmonella*. In contrast, genes associated with the cobalamin biosynthetic process (GO:0009236) were significantly up-regulated, indicating that MicN seems to activate this pathway in some manner. Furthermore, the suppression of aerobic respiration appears to provide a favorable condition for the expression of genes in this pathway[41].

MicN triggers transcriptional reprogramming across multiple life processes in *Salmonella*

We also conducted KEGG enrichment analysis on the differentially expressed genes, identifying a total of 78 pathways, among which 21 were significantly enriched. The enrichment results can be categorized into five groups, with the most prominent pathways related to amino acid biosynthesis, TCA cycle, and fatty acid metabolism (Fig. 3d). The enrichment of these pathways suggests that MicN affects a broad range of primary metabolic pathways, leading to a shift in *Salmonella* towards a low-energy consumption metabolic state, ultimately affecting its replication capacity within macrophages. Results of the KEGG enrichment align well with the GO enrichment and are consistent with the overall trend of downregulation observed in the GO analysis.

To provide a more refined explanation of the impact of MicN on *Salmonella*'s basal metabolism, we mapped the significantly enriched genes to related pathways to explore the genetic basis of this shift (Fig. 4). Initially, we focused on genes encoding components of the respiratory chain, which are responsible for the primary source of cellular energy. Almost all genes involved in the respiratory complex I to complex V were down-regulated. For the TCA cycle, which typically begins with acetyl-CoA, key genes involved in the conversion of pyruvate to acetyl-CoA and the generation of acetyl-CoA from acetate or acetyl-P were all down-regulated, indicating a deficiency in substrates for the TCA cycle. Additionally, the gene encoding citrate synthase (*citA*) and genes involved in the conversion of isocitrate to 2-oxoglutarate and succinate to malate were suppressed, suggesting that the bacteria are in a state of nutritional deficiency. To compensate for this state, ethanolamine is released from the plasma membrane to the cytoplasm by GlpQ and transported to microcompartments (encoded by *eutKLMNS*) by EutH. The microcompartments contain the key genes for ethanolamine utilization, which can break down ethanolamine into NH_3 and acetyl. The acetyl can be used to generate acetyl-CoA, which enters the TCA cycle to replenish the deficiency in acetyl-CoA. The enhanced ethanolamine utilization is accompanied by the synthesis of B12, which is crucial as a cofactor

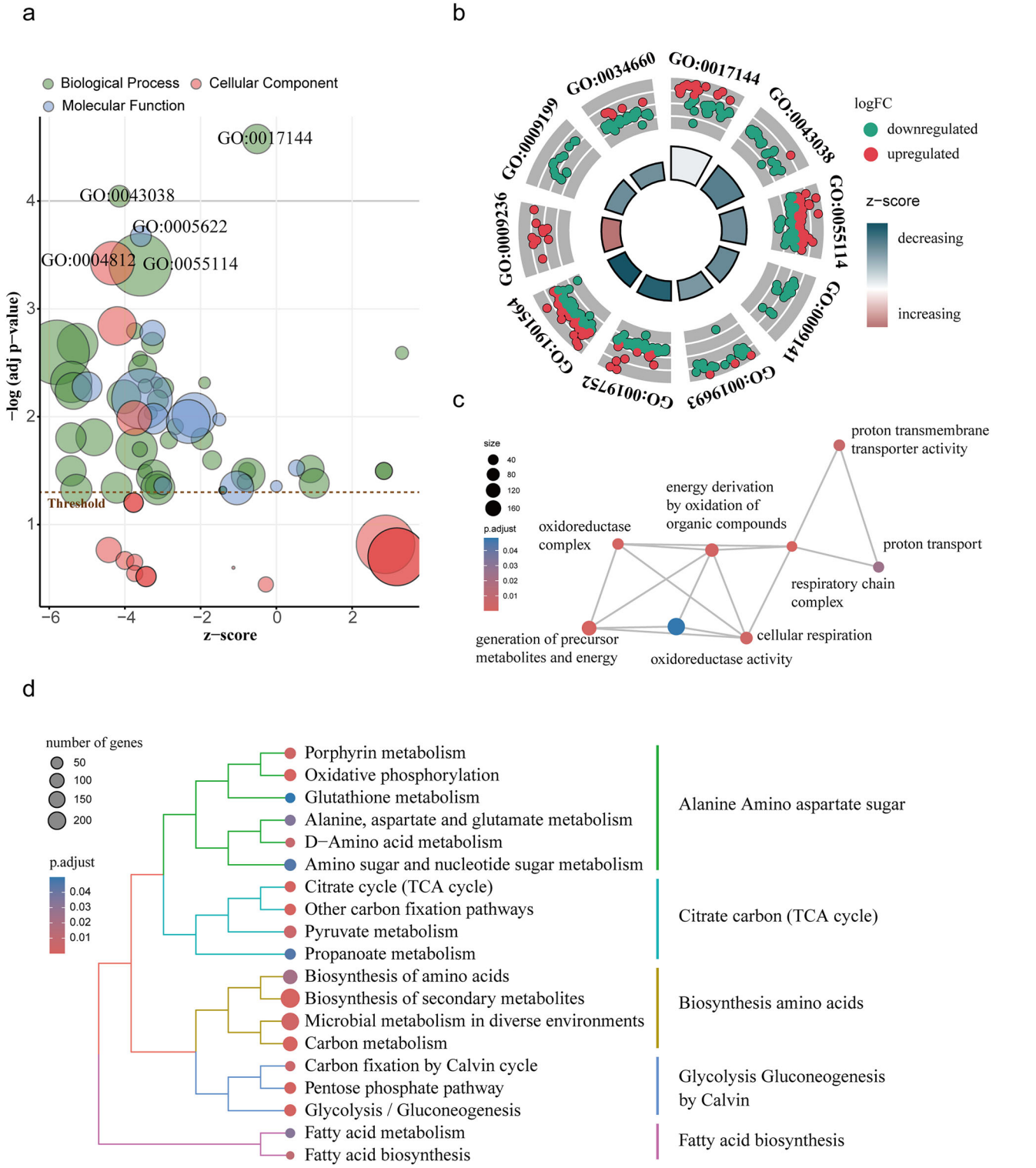

Fig. 3 | Transcriptomic analysis indicates that MicN triggers transcriptional reprogramming in *Salmonella*. Enrichment analyses of Gene Ontology (GO) and Kyoto Encyclopedia of Genes and Genomes (KEGG) annotations for the differentially expressed gene (DEG) sets between p*micN* and Δ*micN*. **a** GO terms for presentation. **b** The top 10 biological process terms identified in the GO enrichment analysis. **c** Network relationships among terms associated with electron transport. **d** Visualization of the top 20 biological processes in a clustered format.

for the activation of the ethanolamine utilization pathway regulatory EutR. Additionally, the cytoplasmic NH_3 seems to increase, as the key genes involved in the conversion of nitrate to NH_3 (nitrate dissimilation reduction pathway) are also up-regulated. The NH_3 can be used to neutralize H^+ in the environment, which is beneficial for *Salmonella* to adapt to the acidic environment with macrophages. As ethanolamine (H_2N-CH_2-CH_2-OH), a key component of phosphatidylethanolamine, is a vital constituent of all cell membranes, the *psp* gene, which is a marker of membrane stress, was also up-regulated as expected[42]. Furthermore, some genes that are beneficial for intracellular colonization, such as *sifA* and *sseL* located on the SPI operon, also showed up-regulated expression. Intriguingly, the metabolic alterations induced by MicN in *Salmonella* closely align with the transcriptional

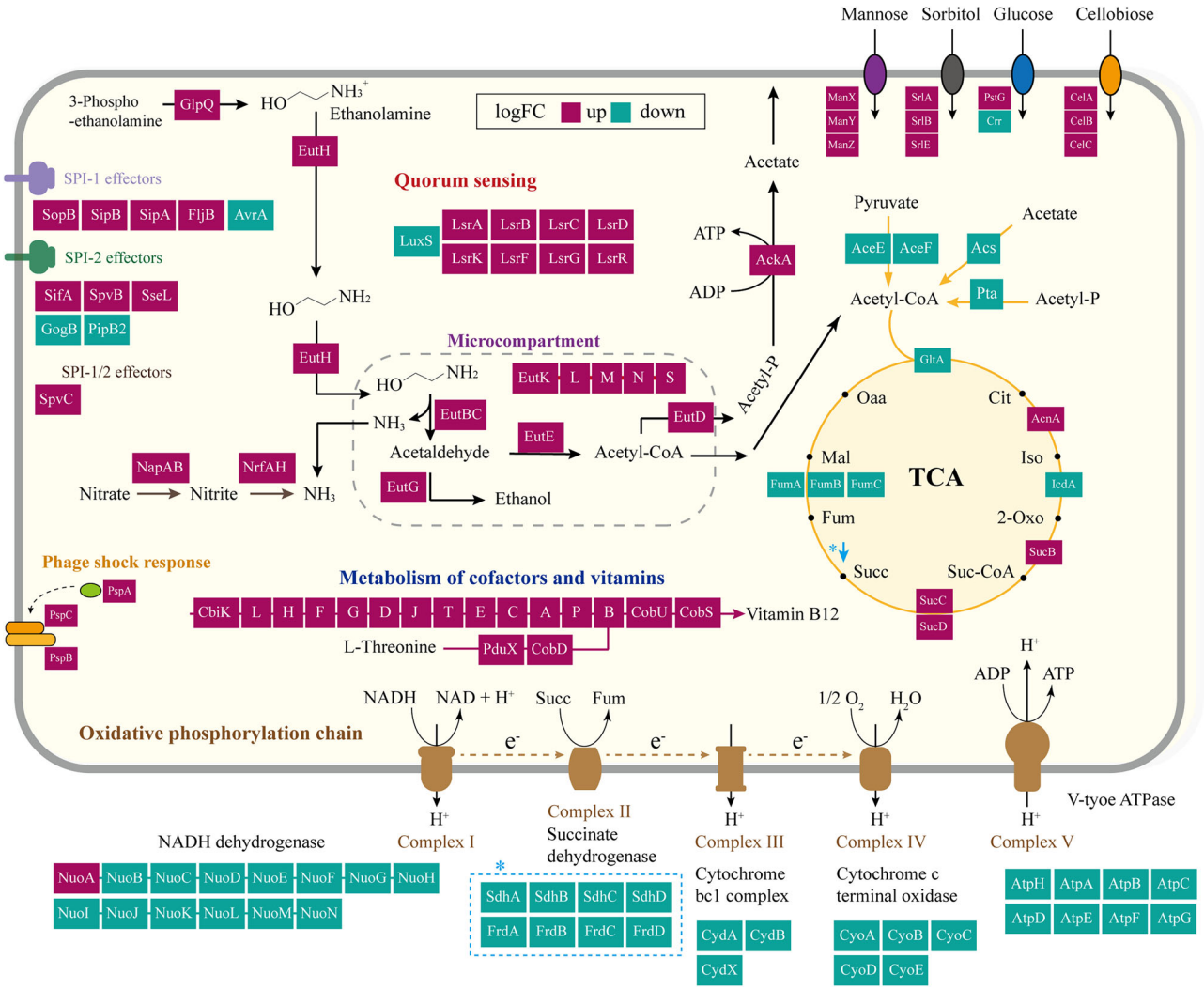

Fig. 4 | Changes in metabolic pathway of *Salmonella* following MicN expression. The expression levels of transcriptomic data are represented by the colors inside the boxes, where upregulation is indicated in purple and downregulation in blue. Genes involved in the respiratory complex I to complex V and the generation of acetyl-CoA in the TCA cycle were down-regulated. Genes for ethanolamine utilization and the synthesis of B12 were up-regulated. Genes located on the SPI operon, which are beneficial for intracellular colonization, also showed up-regulated expression.

changes observed during macrophage invasion[37]. This compelling parallel leads us to propose that MicN serves as a crucial mediator, enabling *Salmonella* to reconfigure its metabolism within macrophages and thereby facilitating its intracellular adaptation.

MicN enhances the expression of genes involved in ethanolamine and 1,2-propanediol utilization pathways

To validate the RNA-sequencing results, seven representative genes (*eutK*, *eutG*, *eutR*, *cobS*, *pduC*, *glpQ*, *pspA*) were further detected in vivo and in vitro using RT-qPCR, with 16S rRNA serving as an internal control (Fig. 5a, b). In alignment with the RNA sequencing data, the transcription levels of *eut*, *cob*, *pdu*, and *pspA* were elevated in vitro following the overexpression of *micN*, compared to the wild type (Fig. 5c). To eliminate the potential influence of the plasmid pBAD24 and arabinose, we also compared the expression of these genes in wild-type and Δ*micN* strains. The comparative analysis of gene expression in minimal M9 medium revealed a consistent pattern of upregulation in the wild-type strain compared to the Δ*micN* strain in vitro (Fig. 5d). To further examine whether *micN*-mediated transcriptional changes occurred during infection, *Salmonella* infection experiments were conducted using RAW264.7 macrophages. Cells were lysed after 4 h of infection, and intracellular bacteria were collected for RNA extraction and gene expression analysis. The results showed that the expression levels of *eut*, *cob*, *pdu*, and *pspA* were significantly up-regulated in wild-type infected cells compared with the Δ*micN* mutant at 4 h post-infection (Fig. 5e).

Overall, MicN exerts varying degrees of influence on the core metabolism of *Salmonella*. The suppression of genes associated with primary metabolism is likely to "dull" the active state of *Salmonella*, promoting a transition to a low-energy metabolic state. This state may provide *Salmonella* with a significant survival advantage under the pressures of antibiotic treatment and within macrophages.

Crystal structure of the functionally uncharacterized *Salmonella* MicN

Due to the absence of homologous structures of MicN in the database, we solved the X-ray crystal structure of MicN using selenium single-wavelength anomalous diffraction at a resolution of 2.3 Å (Fig. 6a, Figure S2, and Table 1). MicN adopts an overall fold comprising five β-stands, designated β-1 to β-5, which collectively form a single antiparallel β-sheet arranged in a barrel-like architecture (Fig. 6b). A flexible loop structure, comprised of residues 26–31, connects β-2 and β-3. MicN is characterized by the presence of six positively charged and nine negatively charged residues, with vacuum electrostatic analysis revealing a higher concentration of negatively charged regions while showing a lower presence of positively charged regions, indicating that this protein is unlikely to function as a DNA-binding protein

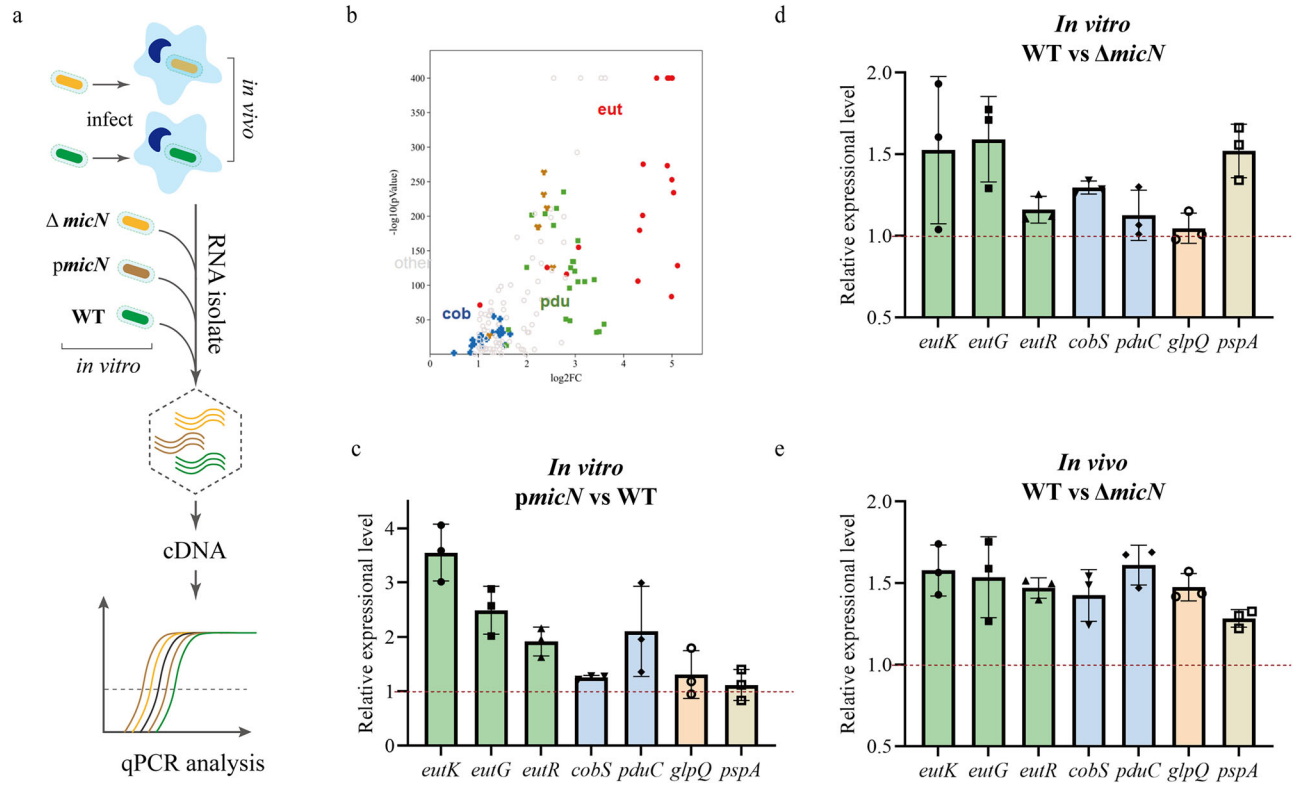

Fig. 5 | In vivo and in vitro validation of changes in the ethanolamine utilization pathway and other representative genes. The mRNA expression levels of seven selected genes (*eutK*, *eutG*, *eutR*, *cobS*, *pduC*, *glpQ*, *pspA*) were analyzed using qRT-PCR. **a** Schematic representation of the experimental flow. **b** Scatter plots were generated to visualize the transcriptomic results. **c** Comparative analysis of gene expression levels in wild-type and p*micN* strains. **d** Comparative analysis of gene expression levels in wild-type and Δ*micN* strains. **e** In vivo qPCR validation conducted on RAW264.7 macrophages infected with wild-type and Δ*micN* strains. Error bars indicate STDEV and mean of at least three independent experiments.

(Fig. 6c, d). Furthermore, we found that MicN could form symmetrical homologous dimers mediated by hydrophobic interactions (Fig. 6e). The specific amino acid residues involved in dimeric interactions were identified from the protein structure and are illustrated (Fig. 6f). The residues Phe5, Trp7, Leu58, Pro60 and Pro61 are in close proximity and contribute to the formation of a relatively stable hydrophobic core.

Highly conserved amino acid residues in homologous proteins often indicate critical functional sites. Therefore, sequence analysis of MicN homologs across diverse species was performed to assess conservation (Fig. 6g). Sequence similarity ranged from 40.32% to 93.55%, with the homolog exhibiting the closest similarity at 80.33% deriving from *Leclercia*. While MicN homologs are distributed across various species, they predominantly cluster within Gama-Proteobacteria, which will be elaborated in subsequent sections. The conserved amino acids identified through sequence alignment are labeled (Fig. 6h), with a significant proportion located at the dimer's junction surface. The distribution and sequence conservation of MicN homologs suggest that MicN plays a vital role in these species. To investigate whether the structure of MicN is similar to that of known structures, we utilized the Dali server to search the PDB database for proteins with structural similarities to MicN; however, no highly homologous structures were identified. Given that the absence of common enzyme-like catalytic or binding domains in the MicN structure, we hypothesize that MicN may function as an auxiliary protein or as an activator/suppressor, influencing the activity of target proteins to exert its biological functions.

MicN interacts with the transcriptional regulatory factor RpoS

After obtaining the structure of MicN, we attempted to identify homologous proteins through structural comparison, but no reliable structural counterparts were detected (Fig. S3). To gain a deeper understanding of the molecular mechanisms underlying the biological function of MicN, we used Z-dock and AlphaFold3 to perform molecular docking based on the protein crystal structure of MicN[43], and the results showed that RpoS was the candidate target protein of MicN (Fig. 7a). From a structural perspective, MicN binds to the N-terminal region of RpoS, covering the σ2.1 regions, with the interaction mediated primarily by hydrogen bonds and salt bridges, allowing the two components to bind in the correct orientation. Several MicN residues (Glu3, Tyr18, Thr20, Leu39, Asp44, Trp7, Arg13, Thr40, Gln41) create hydrogen bonds or salt bridge interactions with residues (Tyr109, Arg108, Lys104, Ala130, Glu76, Leu71, Asn98) of RpoS (Fig. 7b, c). Intriguingly, most of the evolutionarily conserved residues of MicN are clustered at the interface, suggesting a functional relevance of its interaction with RpoS. The surface charge distribution of the MicN-RpoS interface was analyzed subsequently, indicating that the binding surface of the RpoS N-terminal region is predominantly positively charged, while the binding surface of MicN is predominantly negatively charged (Fig. 7a). The opposite polarity of the protein binding surfaces facilitates the stable interaction between the proteins. Given that different sigma factors can exhibit synergistic effects, we analyzed the homology of this interacting region with other sigma factors; however, no homologous regions were detected, and AlphaFold3 analysis did not obtain a high credibility complex structure between MicN and other sigma factors. Therefore, we suppose that MicN does not interact with other sigma factors, or at least not through the same mechanism.

To further validate the interaction between MicN and RpoS, plasmids pUT18C-*micN* and pKNT25-*rpoS* were constructed and co-transformed into *E. coli* BTH101 for bacterial two-hybrid assay. Additionally, *micN* and *rpoS* genes were cloned into the pGL01 vector, with His-tagged MicN serving as bait for pull-down assay. Bio-Layer Interferometry (BLI) was also performed by immobilizing biotinylated RpoS on biosensors, followed by

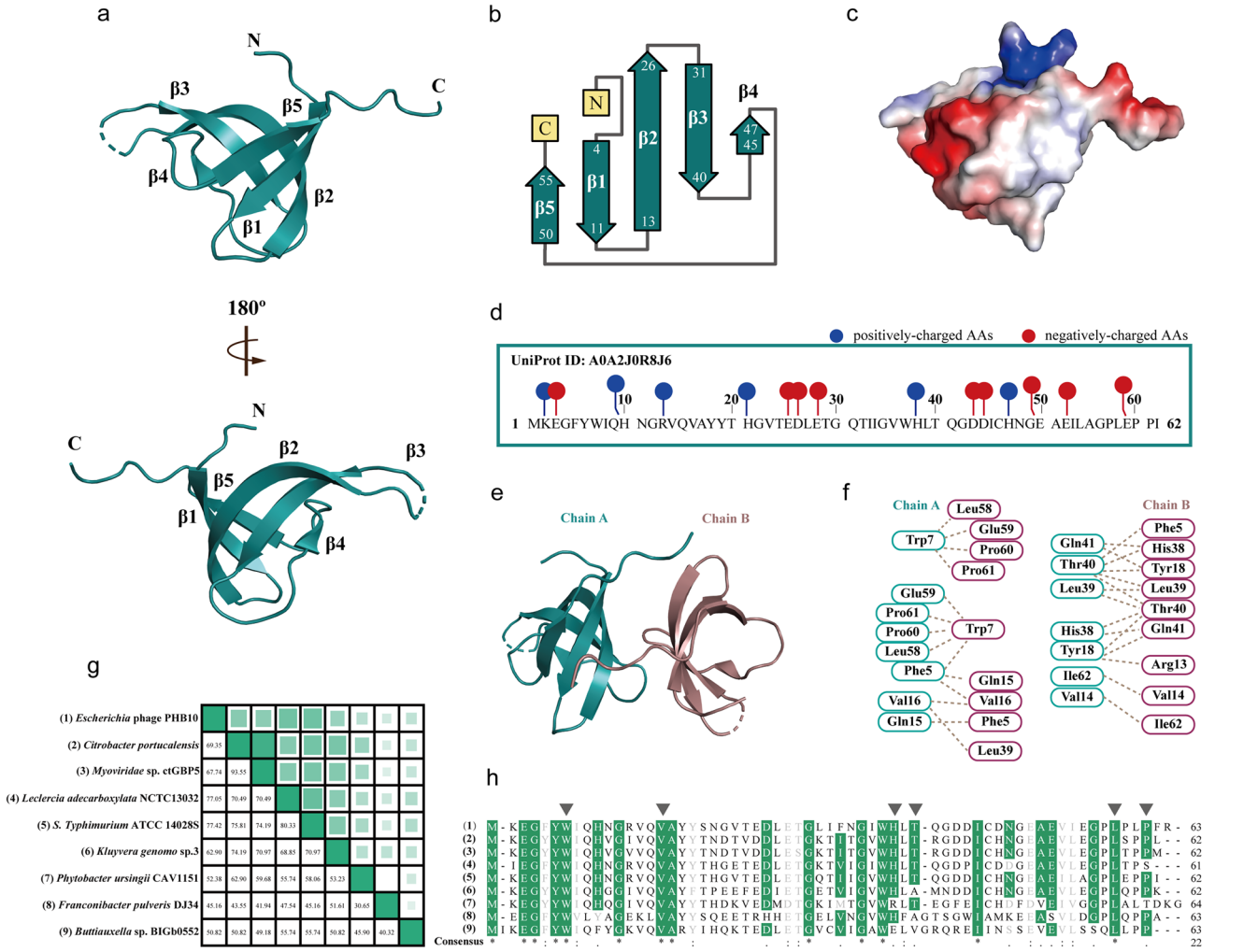

Fig. 6 | Crystal structure of MicN. a Cartoon representation of MicN depicted from two distinct orientations. The N-terminal and C-terminal are indicated by "N" and "C" labels, respectively. Each β-strand in the structure is labeled and numbered for clarity. **b** The topplogy diagram of MicN was generated from the PDB web server and redrawn with the Topo program. **c** Electrostatic surface of MicN generated using APBS, with blue indicating positively charged areas and red representing negatively charged areas. **d** Amino acid sequence of MicN from *S. Typhimurium* 14028S is presented, with positively charged residues denoted by blue balloons and negatively charged residues by red balloons. **e** Analysis of homodimer formation. A cartoon representation of the MicN homodimer, with each chain labeled in blue and pink. **f** Amino acid residues composing the dimer interface. **g** The sequence similarity of MicN across various species is visualized, with blue squares indicating levels of similarity-darker shades and larger squares represent higher sequence similarity. **h** Alignment of MicN sequences from diverse species. Highly conserved residues are highlighted in green.

sequential addition of RNAP and MicN to evaluate binding affinities. Collectively, the results of bacterial two-hybrid assays, in vitro pull-down and BLI assays clearly showed a direct interaction between MicN and RpoS (Fig. 7d–f, and Fig. S4).

MicN disrupts the binding affinity of RpoS to RNA polymerase

We analyzed the genes that exhibited significant changes in expression levels following MicN expression and found that the majority of the up-regulated genes correspond to previously documented RpoS inhibitory proteins (Fig. S5). Consistent with this, Lago's study on Δ*rpoS* also showed a negative correlation between MicN and RpoS[44]. Then we hypothesize that the binding of MicN to RpoS may affect the function of RpoS. RpoS forms a holoenzyme Eσ with the RNAP core by recognizing specific promoters and forming transcription initiation complexes (TICs) to initiate gene transcription[11]. To further clarify the impact of MicN binding to RpoS, we mapped the structure of the MicN-RpoS complex onto the RNAP structure (with a resolution of 3.3 Å; PDB ID code 6OMF) (Fig. 8a). We found that MicN may interfere with the interaction between RpoS and the β′ subunit. A major contribution to the σ-RNAP core association comes from interactions between the σ2 domain and a helix-turn-helix formation, termed a "clamp helices," of the clamp domain of the β′ subunit. MicN creates a significant steric hindrance between RpoS and the β′ subunit, hindering the binding of RpoS to the RNAP core. Furthermore, compared with σ^{70}, which exhibits strong affinity for the RNAP core enzyme (Kd ~0.26 nM), RpoS binds relatively weakly to the RNAP core in the absence of nucleic acids (Kd ~4.26 nM)[18,45]. This suggests that MicN may make it more difficult for RpoS to bind to the core enzyme. Additionally, the Kd value for the interaction between RpoS and MicN is 43.6 nM, an order of magnitude higher than 4.26 nM for RpoS binding to the RNAP core. This indicates that the RpoS-MicN interaction exhibits a lower binding affinity compared to the RpoS-RNAP complex. Consequently, 1 μM MicN was substituted for 0.1 μM RNAP core in BLI assays to compensate for this affinity difference.

To further validate our hypothesis, we designed an experimental scheme based on biosensor interference (Fig. 8b). First, we linked RpoS to the sensor and then assembled it into a holoenzyme complex with core RNAP. Subsequently, we placed this complex in an environment containing MicN to observe the dynamic changes of the large complex. The

experimental results demonstrated that MicN can effectively dissociate the RpoS-RNAP complex, thereby corroborating our hypothesis that MicN functions as an anti-sigma factor for RpoS (Fig. 8c).

Table 1 | X-ray data collection and refinement

Name	Results
Data collection	
Space group	P64
Cell dimensions	
a, b, c (Å)	74.97, 74.97, 65.40
α, β, γ (°)	90.00, 90.00, 120.00
Resolution (Å)	50.00–1.85(2.00–1.85)
Completeness (%)	97.60(100.00)
<I/σ(I)>	16.90(3.00)
Refinement	
Resolution (Å)	37.48–1.86(1.90–1.86)
No. of reflections	15298.00
Rwork (%)	0.21
Rfree (%)	0.26
RMSD bond lengths(Å)	0.85×10^{-2}
RMSD bond angles(°)	1.27
B-factors	22.51
Ramachandran plot (%)	
Most favored	97.98
Allowed	2.02
Outliers	0.00

Discussion

Salmonella is an intracellular pathogen that predominantly resides within the host's macrophages, where various environmental stresses are present. The mechanisms by which *Salmonella* adapts to the challenging conditions of the macrophage environment remain incompletely understood. We have identified a previously uncharacterized small protein, MicN, comprising only 62 amino acids. Our results show that *Salmonella* significantly up-regulates the expression of MicN during survival in macrophages, and the absence of MicN results in a notable reduction in its survival capabilities. This study demonstrates that MicN could significantly improve the survival ability of *Salmonella* in host macrophages and contribute to the formation of persisters under antibiotic stress, providing insights into the mechanisms by which MicN facilitates the intracellular adaptation and antibiotic resistance of *Salmonella*.

To date, 113 small proteins have been identified in *Salmonella*, indicating a possible role in virulence and pathogenicity. Nevertheless, the exact mechanisms by which these proteins exert their effects are still poorly understood. Notably, MicN is mainly distributed in γ-Proteobacteria and is highly conserved in intestinal pathogens, indicating its potential significance in these taxonomic groups (Fig. S3). Furthermore, some genomes of bacteriophages infecting intestinal bacteria also contain MicN encoding genes, suggesting that these phages may serve as intermediary for horizontal gene transfer of *micN*, thereby elucidating the abundance of MicN within the γ-Proteobacteria.

The expression of MicN significantly affects various metabolic processes of *Salmonella*. Several primary metabolic pathways, including the TCA cycle, electron transport and respiratory chain, protein synthesis, nucleotide metabolism, and fatty acid metabolism, are repressed, consistent with previous metabolomic studies, which show that *Salmonella* tends to decrease metabolic rate and utilize lipids as an alternative carbon source to sustain vital activities post-invasion[46]. This shift may represent a significant survival strategy for *Salmonella* in response to adverse conditions.

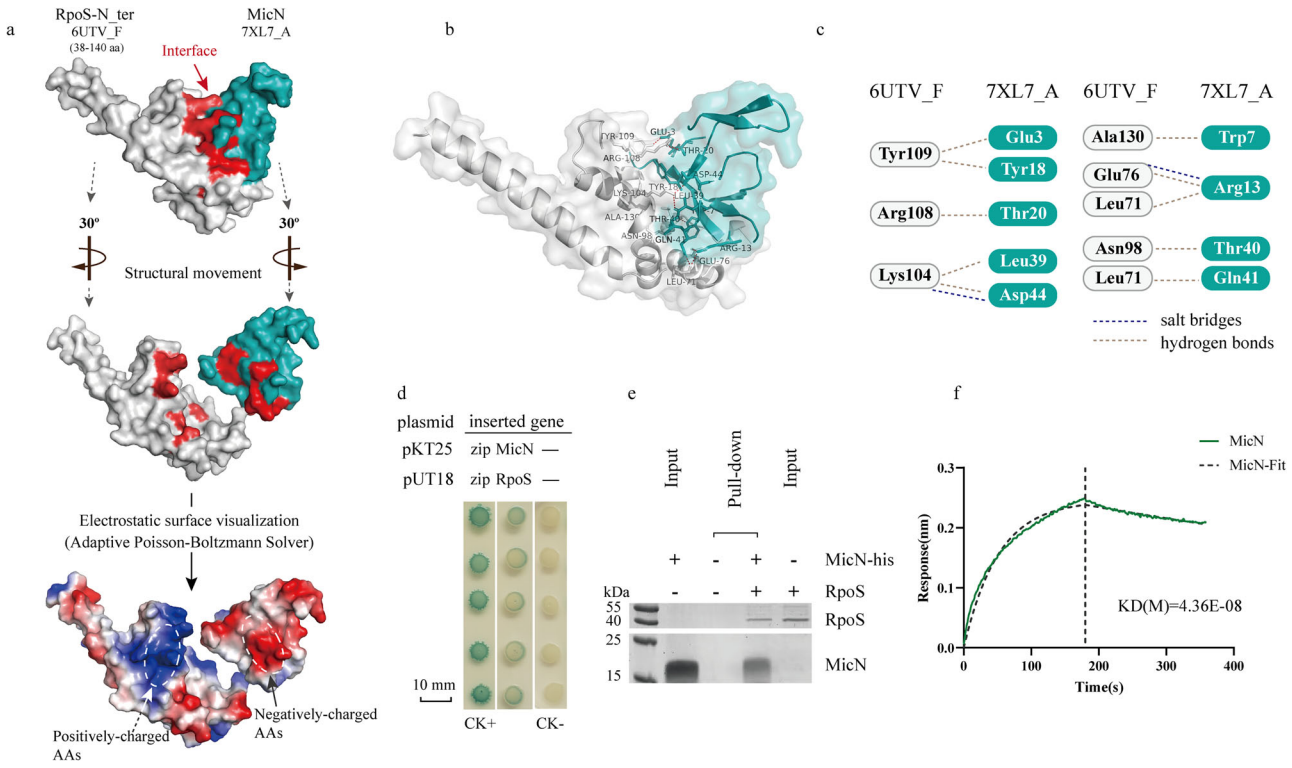

Fig. 7 | Direct interaction between MicN and RpoS. a Surface representation of the MicN-RpoS complex, with MicN shown in blue and RpoS in gray; the interface between MicN and RpoS is highlighted in red. **b**, **c** Amino acid residues composing the complex interface. **d** Bacterial two-hybrid assays confirmed the interactions between MicN and RpoS. **e** Pull-down assays demonstrated the interaction between MicN and RpoS. **f** Fortebio assays demonstrated the interaction between MicN and RpoS.

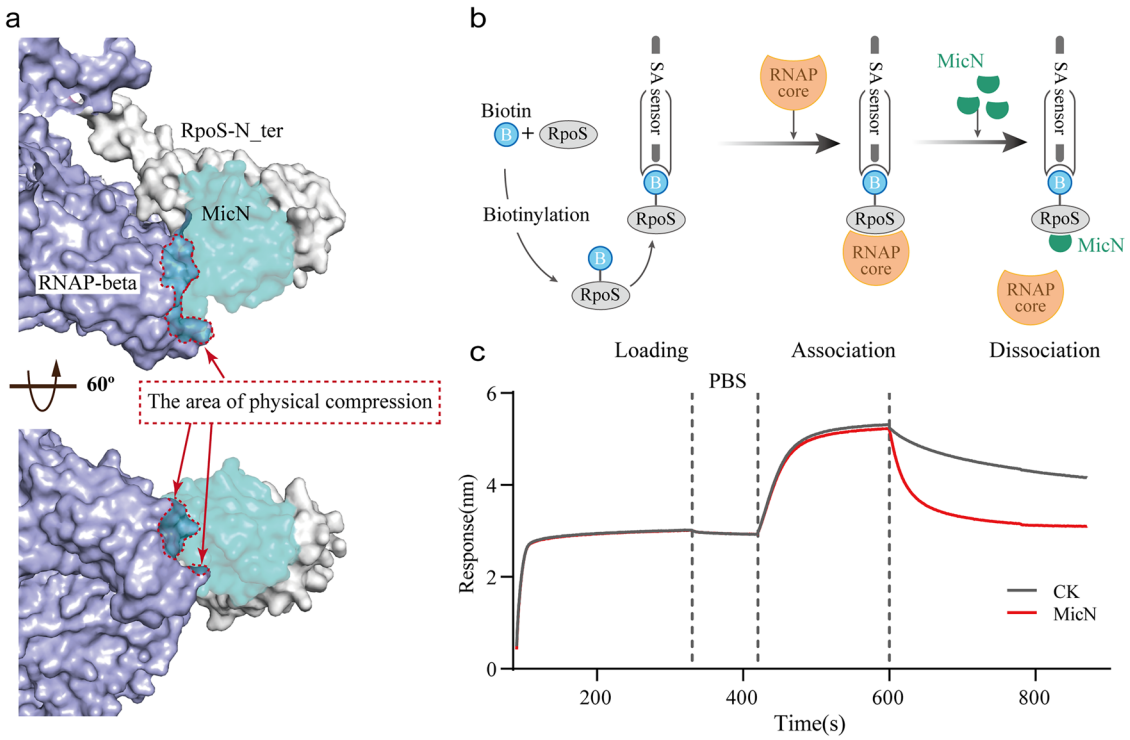

Fig. 8 | MicN binding to RpoS interferes with RpoS binding to β′ subunit. **a** Surface representation of the MicN-RpoS complex mapped onto the RNAP. **b** Schematic representation of the experimental flow of Bio-Layer Interferometry (BLI) approach. **c** Results of BLI show that MicN interferes with the interaction between RpoS and the RNAP.

Furthermore, the utilization of ethanolamine and its associated auxiliary pathways is activated. Ethanolamine, an essential component of lipids, is abundant in the gastrointestinal tract and metabolized via the Eut pathway, resulting in the production of acetyl-CoA and ammonia (NH_3)[47]. Acetyl-CoA enters the TCA cycle for energy production, providing a crucial carbon supplement for intracellular environments where carbon availability is restricted. Concurrently, NH_3 serves to neutralize protons in the cytoplasm, effectively counteracting the acidic conditions present in macrophages. This adaptive mechanism for counteracting low pH is reminiscent of the strategy employed by *Helicobacter pylori*, which utilizes urease to produce NH_3, thereby neutralizing surrounding H^+[48]. Moreover, phosphatidylethanolamine, components of cell membranes, are up-regulated in *Salmonella* for the utilization of these metabolites, which is advantageous for nutrient acquisition and intracellular survival. A critical stage of *Salmonella* pathogenesis involves colonization within the mammalian gastrointestinal tract, which requires the catabolism of a number of carbon sources. The *eut* and *pdu* clusters play a vital role in this catabolism and facilitate the adaptation of bacteria to specific anaerobic environments. Resident microbiota are poorly equipped to metabolize ethanolamine, and *Salmonella* exploits ethanolamine utilization to avoid nutritional competition in establishing infection. A diverse array of gut microbes, including *Salmonella*, *Escherichia*, *Enterococcus*, and *Clostridium*, have the capacity to utilize ethanolamine as their exclusive source of carbon, nitrogen, and energy, thereby occupying a specialized niche or establishing infection[49]. We present a model wherein the invasion of *Salmonella* into macrophages results in a pronounced upregulation of MicN. This elevated expression disrupts the interaction between RpoS and the core RNA polymerase, inducing significant alterations in *Salmonella*'s gene expression profile. Consequently, previously suppressed gene clusters, such as *eut* and *pdu*, are activated, enabling transcriptional reprogramming that allows *Salmonella* to rapidly adapt to the hostile intracellular conditions of macrophages (Fig. 9).

RpoS is a key regulator of stress responses in numerous Gram-negative bacteria, playing a crucial role in protecting organisms from adverse conditions. It is also implicated in the virulence, pathogenicity, and antibiotic tolerance of various pathogens. RpoS broadly regulates the expression of hundreds of genes, yet the mechanisms by which bacteria precisely and selectively activate specific genes under different stress conditions remain unclear. We identified MicN as a regulatory factor of RpoS. MicN influences RpoS binding to RNAPs, thereby changing the expression profile of *Salmonella*. RpoS plays a critical role in bacterial survival under stress conditions; however, bacteria must navigate a trade-off between resisting environmental pressures and promoting growth. For instance, RpoS can inhibit the expression of SPI-2 genes, which are vital for *Salmonella*'s survival and replication within macrophages. Consequently, *Salmonella* has developed an intricate regulatory network that meticulously controls RpoS at the levels of transcription, translation, and post-translational modification. A key mechanism in regulating RpoS binding to the core RNAP to initiate transcription involves the anti-sigma factor, which can physically obstruct the binding interface between RpoS and RNAP or interfere with their interaction. Once the inhibition by the anti-sigma factor is lifted, RpoS can promptly initiate the expression of downstream genes. Our findings indicate that MicN functionally resembles anti-sigma factors. The interaction between MicN and the N-terminus of RpoS establishes a spatial barrier that inhibits RpoS from associating with the β′ subunit of RNA polymerase. The binding of MicN to RpoS affects its normal function, leading to shifts in the gene set regulated by RpoS during transcription initiation. By transiently inhibiting RpoS activity, MicN facilitates the restoration of metabolic pathways that RpoS typically represses, including ethanolamine and propionate utilization. This restoration not only supplies energy for *Salmonella* but also aids in neutralizing H^+, thereby enhancing intracellular adaptability. Consequently, MicN is a significant component of the RpoS feedback regulatory network, playing an essential role in the intracellular adaptability and replication of *Salmonella*. Overall, the interaction between MicN and RpoS leads to widespread alterations in gene expression patterns, thereby regulating the expression of specific genes associated with intracellular adaptation in *Salmonella*, which confers a significant advantage for rapid adaptation to hostile environments.

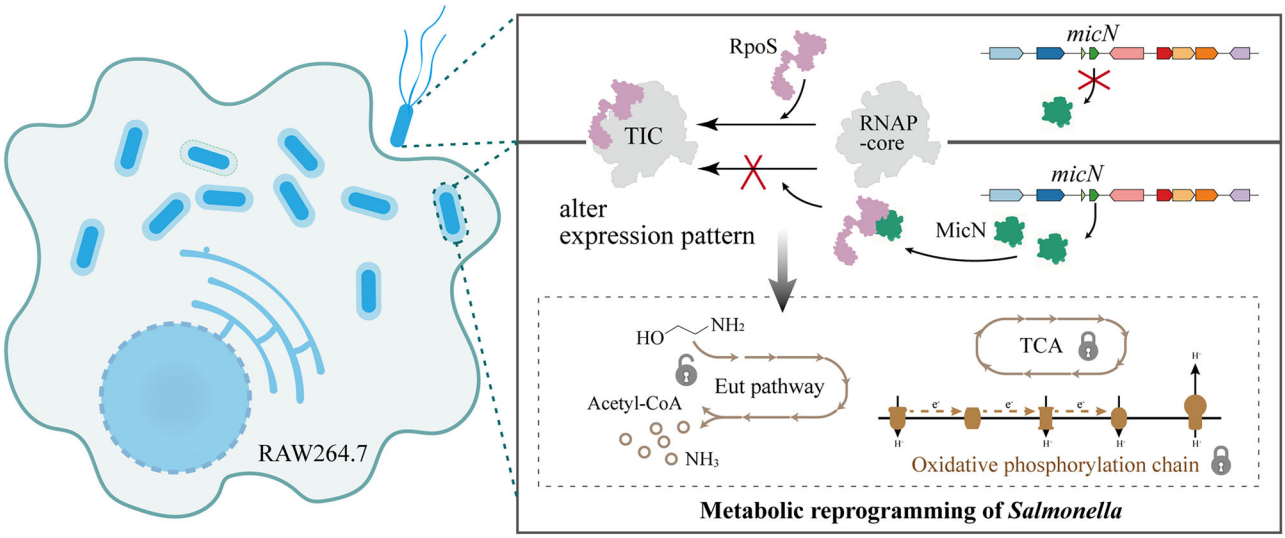

Fig. 9 | Model of MicN-mediated regulatory mechanism in *Salmonella*. During macrophage infection, *Salmonella* produces the small protein MicN, which interacts with the target protein RpoS and modulates its binding to RNAP. This interaction leads to the transcriptional reprogramming of *Salmonella* and allows *Salmonella* to adopt a low-energy metabolic strategy, thereby improving its adaptability within intracellular environments.

In summary, we have identified MicN, a previously uncharacterized small protein, and delved into its structure, function, and mechanism of action. Our findings reveal that MicN enhances the adaptation and survival of *Salmonella* by interacting with RpoS, providing supplementary insights into the regulatory mechanisms of RpoS and the intracellular adaptation strategies of *Salmonella*. Although small proteins are known to play diverse roles in bacterial physiology, their importance has often been obscured by insufficient genome annotations[38]. Our research provides a reference for the functional exploration of other small proteins. Additionally, the structural data obtained for MicN lays a foundational basis for future drug design efforts. While our work underscores the critical role of MicN in *Salmonella*, the precise mechanisms by which *Salmonella* senses and adapts to the intracellular environment of host cells to improve survival remain to be fully elucidated. This finely tuned regulatory mechanism in *Salmonella* confers a survival advantage in diverse environments. Current research indicates that MicN confers environmental adaptive advantages to *Salmonella* through a sophisticated multi-tiered regulatory network: At the transcriptional level, *micN* exhibits a stringent stress-responsive pattern-showing significant upregulation within macrophages and under carbon starvation conditions while remaining silent during normal growth, with this dynamic expression closely linked to bacterial survival states. Lago et al. further demonstrated markedly reduced MicN (STM14_3199) expression in Δ*rpoS* mutant, indicating that RpoS can also affect the expression of MicN[44]. Combined with the finding that MicN inhibits the function of RpoS through protein-protein interactions, we propose a feedback regulatory mechanism of RpoS operating at the protein level. Both RpoS and MicN exist in a dynamic equilibrium. Upon exposure to adverse conditions, RpoS, the key regulator of the stress response, is rapidly expressed and concurrently promotes the expression of MicN. The accumulation of MicN serves to mitigate the excessive expression of RpoS, positioning it as a crucial component of the dynamic regulatory mechanism governing RpoS. Furthermore, structural analysis reveals that MicN can form dimers, which encapsulate the interaction interface with RpoS within the dimeric structure. The structural configuration prevents the dimer from binding to RpoS, thereby inhibiting the activity of MicN. We hypothesize that under conditions where RpoS is required, existing MicN proteins dimerize to alleviate the inhibition on RpoS, allowing RpoS to rapidly activate its stress response functions. However, we have yet to identify the specific upstream regulator that triggers MicN expression, and we anticipate that future research will provide deeper insights into this mechanism. This intricate regulatory network presents a compelling avenue for further investigation.

Material and Methods

Bacterial strains, media and culture conditions

S. Typhimurium ATCC 14028S and its derivatives were cultivated in standard liquid Luria Bertani (LB) medium (containing tryptone, 10 g/L; NaCl, 5 g/L; yeast extract, 5 g/L) or M9 minimal medium (Na_2HPO_4, 6.78 g/L; KH_2PO_4, 3 g/L; NaCl, 0.5 g/L; NH_4Cl, 1 g/L; $MgSO_4$, 0.241 g/L; $CaCl_2$, 0.011 g/L; glucose, 4 g/L) at 37 °C. For the antibiotic tolerance test, bacteria were grown in M9 minimal medium to an optical density of 0.3 at 600 nm (OD_{600}) with shaking, followed by the addition of gentamicin (50 μg/mL, Solarbio) or colistin (40 μg/mL, Solarbio).

In this study, three distinct *E. coli* strains were employed: (i) BL21(DE3) for protein expression and purification, (ii) DH5α for strain engineering and genetic modifications, and (iii) BTH101 for bacterial two-hybrid systems. All strains were cultivated in LB medium, with ampicillin (100 μg/mL, Solarbio), kanamycin (50 μg/mL, Solarbio), X-Gal (40 μg/mL, Coolaber), and IPTG (0.5 mM/mL, Solarbio) being supplemented as needed.

Construction of *micN* derivative strain

The *micN* gene knockout strain was constructed using the lambda Red recombinase system as described previously[50]. For the construction of *micN* over-expressing strain, *S. Typhimurium STM14_RS14310* was cloned into the pBAD24 vector, which is an arabinose-induced expression plasmid. To further elucidate the role of MicN and its effect on the expression of key genes in *Salmonella*, a pBAD24-*micN* vector designed for robust and inducible expression of the *micN* gene was constructed and introduced into the Δ*micN* strain (denoted as p*micN*), allowing the analysis of the transcriptomes under high *micN* expression levels (Fig. S6). As a control, the original plasmid pBAD24 was also introduced into the Δ*micN* strain. Arabinose was added to a final concentration of 0.05% to induce the expression of p*micN*. Primers and plasmids used in this study are listed in Table S1 and Table S2.

Growth curves

S. Typhimurium ATCC 14028S and the derivative strain Δ*micN* were cultured overnight in LB with shaking (180 rpm) at 37 °C to ensure optimal growth conditions. Following the overnight incubation, the bacterial cultures were diluted 1:100 into fresh LB or M9 minimal medium and further incubated with continuous shaking at 37 °C. The bacterial growth was monitored by measuring the optical density at 600 nm (OD_{600}) using a Bioscreen C Automatic Growth Analyzer, with readings taken every 30 min for accurate quantification. All strains were performed with four replicates.

Macrophage infection models

The RAW264.7 macrophage cell line was obtained from Ubigene (Guangzhou, China). For the infection experiments, *S. Typhimurium* strains were inoculated in LB medium overnight at 37 °C with agitation. The culture was then diluted 1:100 into M9 minimal media and further incubated at 37 °C to the mid-exponential phase (OD_{600} = 0.5) for *micN* expression. RAW264.7 cells were cultured in Dulbecco's Modified Eagle Medium (DMEM, Gibco) medium supplemented with 10% fetal bovine serum (FBS, Gibco). Approximately 1×10^5 cells were seeded into each well of a 96-well plate and incubated at 37 °C in a humidified environment with 5% (v/v) CO_2. Cells were then infected with wild-type *Salmonella* and Δ*micN* at a multiplicity of infection (MOI) of 10. After 1 h of infection, the cells were washed twice with PBS, and fresh DMEM medium containing gentamicin (100 μg/mL) or ampicillin (20 μg/mL) was added to eliminate extracellular bacteria. Cell samples were collected at specific time points (2, 4, 6, and 8 h post-infection), lysed in 1% Triton X-100, subjected to gradient dilution, and plated on LB Agar for colony-forming unit (CFU) counting. For gene expression analysis of seven representative genes (*eutK*, *eutG*, *eutR*, *cobS*, *pduC*, *glpQ*, *pspA*), cells were washed after infection for 4 h and lysed in 1% Triton X-100 for RNA extraction. Bacteria before invasion were used as controls (0 h) to compare the expression levels before and after infection.

Invasion assay

The HT-29 cell line was obtained from Ubigene (Guangzhou, China) and cultured in RPMI-1640 medium (Gibco) supplemented with 10% FBS. Cells were incubated at 37 °C in a humidified environment with 5% (v/v) CO_2. Wild-type and Δ*micN* cultures were centrifuged to harvest the bacteria, which were then diluted with RPMI-1640 medium and seeded on confluent HT-29 cells in 96-well plates at an infection multiplicity of 10. One hour after infection, gentamicin (100 μg/mL) was added to the cells for 1 h to eliminate extracellular bacteria. The cells were gently washed with phosphate-buffered saline (PBS, Gibco) and subsequently disrupted using 1% Triton X-100. The number of intracellular bacteria was determined by counting the CFU of viable colonies.

LDH assay

The cytotoxic effects of *Salmonella* were assessed using the Promega CytoTox 96 Nonradioactive Cytotoxicity Assay Kit, which quantitatively measures lactate dehydrogenase released from lysed mammalian cells via a coupled enzymatic assay. The RAW264.7 macrophage cell line was cultivated in DMEM fortified with 10% FBS for optimal growth, maintained at 37 °C with 5% (v/v) CO_2. Cells were seeded in 96-well plates at a density of 1×10^5 cells per well, and logarithmically growing bacterial cultures were introduced to the cells with an infection multiplicity of 10. Four hours after infection, the supernatants were collected, and freshly prepared reagents were added. The absorbance at 490 nm (OD_{490}) was measured after a 30 min incubation in the dark at room temperature, and the percentage of cytotoxicity was quantitatively determined.

Murine infection models

All animal experiments were approved by the Animal Care and Use Ethics Committee of the Institute of Basic Medicine, Shandong Academy of Medical Sciences (IBMSAMSC Number 098). We have complied with all relevant ethical regulations for animal use. Six to eight-week-old female C57BL/6 mice were purchased from Pengyue Technology Co., Ltd. (Jinan, China) and maintained under specific pathogen-free conditions at 25 °C. After one week of acclimatization, animals were randomly divided into two groups (n = 6 per group). Each mouse was administered 2×10^5 cells of either wild-type or Δ*micN* via intraperitoneal injection, using a 100 μL volume of PBS. Survival rates were recorded at three-hour intervals, and the resulting data were plotted to generate survival curves. All observations were included in the analysis without data exclusion.

RNA-seq and data analysis

Strains carrying plasmids pBAD24-*micN* and pBAD24 respectively, were grown in LB medium supplemented with 100 μg/mL ampicillin and 0.05% arabinose at 37 °C to an OD_{600} of approximately 0.4, then centrifuged at 6000 rpm for 5 min. The resulting bacterial precipitate was promptly flash-frozen in liquid nitrogen. Three independent biological replicates were prepared for each strain. Transcriptome sequencing was performed on an Illumina HiSeq™ 4000 platform using the services of Novogene Technology Co. Ltd. (Beijing, China). Clean reads were obtained by removing low-quality reads and reads containing adapters and ploy-N from raw reads using SOAPnuke software[51]. The filtered reads were then mapped to the reference *S. Typhimurium* ATCC 14028S genome (Genome ID: NC_016856.1) available from the NCBI database, using HISAT 2.1.0 software. Gene expression levels were quantified using RSEM software (version 1.2.8), employing the FPKM method to represent gene expression[52,53]. Differential gene expression (DGE) analysis was conducted with EdgeR employing TMM normalization, and DEGs were defined as having a p-value < 0.05 and a $|\log_2(\text{FoldChange})| > 1$ compared to the control groups. The identified DEGs were annotated against the Gene Ontology (GO) and Kyoto Encyclopedia of Genes and Genomes (KEGG) databases, followed by GO term functional analysis and KEGG pathway enrichment analysis[54,55].

RNA preparation and real-time quantitative PCR

The wild-type and Δ*micN* strains were cultured in M9 minimal media at 37°C until reaching the mid-exponential phase (OD_{600} = 0.5) for RNA extraction. For in vivo assays, bacteria were added to RAW264.7 cells at an MOI of 10. After 4 h of infection, cells were washed and lysed in 1% Triton X-100 for RNA extraction. Total RNA extraction was performed using the RNAprep Pure Cell/Bacteria Kit (Tiangen Biotech). RNA was subsequently reverse transcribed to cDNA using the Vazyme HiScript III 1st Strand cDNA Synthesis Kit according to the manufacturer's instructions and quantified using a NanoDrop 2000 instrument (Thermo Fisher Scientific). Primers for real-time quantitative PCR were designed based on target gene sequences from *S. Typhimurium* ATCC 14028S, and primer pairs were identified using the National Center for Biotechnology Information (NCBI) PrimerBLAST. The resulting cDNA samples were assayed using a real-time quantitative PCR assay at Applied Biosystems 7500. Relative expression levels of the target genes were calculated using the 2 -ΔΔCT method described by Livak et al., and 16sRNA was used as an internal control. Data were analyzed using Origin 9.1 (Origin Lab Corporation)[56].

Protein expression and purification

The *micN* and *rpoS* genes were amplified from *S. Typhimurium* ATCC 14028S genomic DNA and cloned into the expression vector pGL01. Protein expression was carried out in the *E. coli* BL21(DE3) strain. Cultures were gradually cooled to 16 °C when the OD_{600} reached 0.4-0.6, and induction was achieved by adding 0.1 mM IPTG. Cells were harvested at 4000 rpm for 20 min. A sonication process was employed for 10 min, consisting of 3 s pulses separated by 5 s intervals, for protein lysis. Purification involved a sequential process: Ni^{2+}-NTA affinity chromatography, anion exchange chromatography, and gel filtration chromatography. The His-tag was cleaved off using PPase[57]. Proteins were further concentrated and refined through Superdex 200 chromatography. Protein quality and concentration were assessed using sodium dodecyl sulphate-polyacrylamide gel electrophoresis (SDS-PAGE), complemented by Coomassie blue staining. All purification procedures were performed at a constant 4°C to maintain optimal conditions.

Bacterial two-hybrid assay

Plasmids of pUT18C-*micN* and pKNT25-*rpoS* were constructed using the Bacterial Adenylate Cyclase Two-Hybrid System Kit (BACTH System Kit, Euromedex, EUK001), and co-transformed into the *E. coli* BTH101 strain. In addition, pKNT25 and pUT18C were introduced into BTH101 as a negative control. Positive, negative, and target strains were cultivated to logarithmic growth phase in LB medium containing 100 μg/mL ampicillin,

50 μg/mL kanamycin, and 0.5 mM/mL IPTG, then 2 μL of each sample was plated onto the LB plates containing 100 mg/mL ampicillin, 50 mg/mL kanamycin, 0.5 mM IPTG, and 40 mg/mL X-Gal.

Pull-down assay

Genes of *micN* and *RpoS* were amplified from *S. Typhimurium* ATCC 14028S genomic DNA and cloned into the pGL01 vector, which is a modified expression vector based on pET15b with a PPase cleavage site to remove the His tag. MicN with a his-tag was used as bait protein, and RpoS without the his-tag was used as the prey protein. The two proteins were subjected to ultrasonic fragmentation, incubated on a nickel column, and subsequently separated by SDS-PAGE. Prey proteins were incubated with Ni^{2+}-NTA beads alone as a negative control.

Bio-Layer Interferometry assay

Bio-Layer Interferometry experiments were performed using an Octet RED96 instrument (ForteBio) at 25 °C. Biotinylated RpoS (0.1 μM) was immobilized on SuperStreptavidin sensors (ForteBio, 18-5057) after incubation with EZ-Link-Biotin at 25 °C for 30 min, and then 0.1 μM RNAP (New England Biolabs, M0550S) was loaded onto each sensor in PBS. To study the effect of MicN on the interaction between RpoS and RNAP, 1 μM of purified MicN was added to displace RNAP core, with an equal amount of PBS added as a control. Data were processed by deduction with sensor control.

Protein crystallization and structure determination

Crystals of MicN were grown using the hanging drop vapor diffusion method at 16 °C in a buffer solution containing 1.2 M lithium sulfate monohydrate and 0.1 M 1,3-Bis-Tris propane at pH 7.0. Diffraction data were collected at the Shanghai Synchrotron Radiation Facility (SSRF) using beamlines BL17u1 and BL19ul, and subsequently processed with HKL2000 software[58–60]. For cryoprotection, crystals were soaked in mother liquor supplemented with 20% (v/v) glycerol. Structural figures were generated using PyMol software (https://pymol.org/2/). Due to the absence of homologous structures and the presence of only a single methionine residue in MicN, Leu27 and Ile33 were mutated to methionine to facilitate the determination of crystallographic phases. The mutated gene was subsequently ligated into the plasmid pGL01 and transformed into *E. coli* BL21. Protein purification was conducted following the established MicN protocol. Specifically, when the OD_{600} reached 0.4–0.6, L-Leucine, L-Isoleucine, L-Valine, L-Lysine, L-Threonine, L-Phenylalanine, and L-Selenomethionine were added to the culture at a concentration of 50 mg/L.

Statistical analysis

All analyses were conducted using GraphPad Prism, and a two-tailed Student's t-test was used to calculate the *p*-value. The statistical significance was denoted as $^{***}p < 0.001$, $^{**}p < 0.005$, $^{*}p < 0.05$. Each experiment was repeated at least three times.

Reporting summary

Further information on research design is available in the Nature Portfolio Reporting Summary linked to this article.

Data availability

The data that support the findings of this study are available from Bingqing Li (bingqingsdu@163.com), upon reasonable request. Original data is available in Mendeley Dataset (doi: 10.17632/9jxhzr8f59.1). Structure of MicN is available in Protein Data Bank under accession number 7XL7. The raw sequence data reported in this paper have been deposited in the Genome Sequence Archive in National Genomics Data Center[61,62], China National Center for Bioinformation/Beijing Institute of Genomics, Chinese Academy of Sciences (GSA: CRA020931), which are publicly accessible at https://ngdc.cncb.ac.cn/gsa. Results of RNA-Seq analysis is available in Supplementary Data.

Received: 15 April 2025; Accepted: 30 September 2025;
Published online: 23 October 2025

References

1. Hallstrom, K. N. & McCormick, B. A. The type three secreted effector SipC regulates the trafficking of PERP during *Salmonella* infection. *Gut Microbes* **7**, 136–145 (2016).
2. LaRock, D. L., Chaudhary, A. & Miller, S. I. Salmonellae interactions with host processes. *Nat. Rev. Microbiol* **13**, 191–205 (2015).
3. Gogoi, M., Shreenivas, M. M. & Chakravortty, D. Hoodwinking the big-eater to prosper: the *Salmonella*-macrophage paradigm. *J. Innate Immun.* **11**, 289–299 (2019).
4. Liu, X. et al. *Salmonella enterica* serovar Typhimurium remodels mitochondrial dynamics of macrophages via the T3SS effector SipA to promote intracellular proliferation. *Gut Microbes* **16**, 2316932 (2024).
5. Haraga, A., Ohlson, M. B. & Miller, S. I. Salmonellae interplay with host cells. *Nat. Rev. Microbiol* **6**, 53–66 (2008).
6. Sholpan, A., Lamas, A., Cepeda, A. & Franco, C. M. *Salmonella* spp. quorum sensing: an overview from environmental persistence to host cell invasion. *AIMS Microbiol* **7**, 238–256 (2021).
7. Fang, F. C., Frawley, E. R., Tapscott, T. & Vazquez-Torres, A. Bacterial stress responses during host infection. *Cell Host Microbe* **20**, 133–143 (2016).
8. Pradhan, D. & Devi Negi, V. Stress-induced adaptations in *Salmonella*: a ground for shaping its pathogenesis. *Microbiol Res*. **229**, 126311 (2019).
9. Nyström, T. Growth versus maintenance: a trade-off dictated by RNA polymerase availability and sigma factor competition?. *Mol. Microbiol* **54**, 855–862 (2004).
10. Feklístov, A., Sharon, B. D., Darst, S. A. & Gross, C. A. Bacterial sigma factors: a historical, structural, and genomic perspective. *Annu Rev. Microbiol* **68**, 357–376 (2014).
11. Österberg, S., del Peso-Santos, T. & Shingler, V. Regulation of alternative sigma factor use. *Annu Rev. Microbiol* **65**, 37–55 (2011).
12. Battesti, A., Majdalani, N. & Gottesman, S. The RpoS-mediated general stress response in *Escherichia coli*. *Annu Rev. Microbiol* **65**, 189–213 (2011).
13. Lange, R. & Hengge-Aronis, R. Identification of a central regulator of stationary-phase gene expression in *Escherichia coli*. *Mol. Microbiol* **5**, 49–59 (1991).
14. Wong, G. T. et al. Genome-Wide Transcriptional Response to Varying RpoS Levels in *Escherichia coli* K-12. *J. Bacteriol.* **199**, e00755–16 (2017).
15. Cho, B. K., Kim, D., Knight, E. M., Zengler, K. & Palsson, B. O. Genome-scale reconstruction of the sigma factor network in *Escherichia coli*: topology and functional states. *BMC Biol.* **12**, 4 (2014).
16. Robbe-Saule, V. et al. Crl activates transcription initiation of RpoS-regulated genes involved in the multicellular behavior of *Salmonella enterica* serovar Typhimurium. *J. Bacteriol.* **188**, 3983–3994 (2006).
17. Dong, T. & Schellhorn, H. E. Role of RpoS in virulence of pathogens. *Infect. Immun.* **78**, 887–897 (2010).
18. Xu, J. et al. Crl activates transcription by stabilizing active conformation of the master stress transcription initiation factor. *Elife* **8**, e50928 (2019).
19. Stewart, P. S. et al. Contribution of stress responses to antibiotic tolerance in *Pseudomonas aeruginosa* biofilms. *Antimicrob. Agents Chemother.* **59**, 3838–3847 (2015).
20. Wu, N. et al. Ranking of persister genes in the same *Escherichia coli* genetic background demonstrates varying importance of individual persister genes in tolerance to different antibiotics. *Front Microbiol* **6**, 1003 (2015).

21. Valencia, E. Y., de Moraes Gomes, F., Ospino, K. & Spira, B. RpoS role in antibiotic resistance, tolerance and persistence in *E. coli* natural isolates. *BMC Microbiol* **24**, 72 (2024).
22. Hong, S. H., Wang, X., O'Connor, H. F., Benedik, M. J. & Wood, T. K. Bacterial persistence increases as environmental fitness decreases. *Micro. Biotechnol.* **5**, 509–522 (2012).
23. Klauck, E., Typas, A. & Hengge, R. 2007. The sigmaS subunit of RNA polymerase as a signal integrator and network master regulator in the general stress response in *Escherichia coli*. *Sci. Prog.* **90**, 103–127 (2007).
24. Cavaliere, P. & Norel, F. Recent advances in the characterization of Crl, the unconventional activator of the stress sigma factor σS/RpoS. *Biomol. Concepts* **7**, 197–204 (2016).
25. Cavaliere, P. et al. Binding interface between the *Salmonella* σ(S)/RpoS subunit of RNA polymerase and Crl: hints from bacterial species lacking *crl*. *Sci. Rep.* **5**, 13564 (2015).
26. Robbe-Saule, V., Lopes, M. D., Kolb, A. & Norel, F. 2007. Physiological effects of Crl in *Salmonella* are modulated by sigmaS level and promoter specificity. *J. Bacteriol.* **189**, 2976–2987 (2007).
27. Paget, M. S. Bacterial Sigma Factors and Anti-Sigma Factors: Structure, Function and Distribution. *Biomolecules* **5**, 1245–1265 (2015).
28. Ilag, L. L. et al. Mass spectrometry of *Escherichia coli* RNA polymerase: interactions of the core enzyme with sigma70 and Rsd protein. *Structure* **12**, 269–275 (2004).
29. Westblade, L. F. et al. Studies of the *Escherichia coli* Rsd-sigma70 complex. *J. Mol. Biol.* **335**, 685–692 (2004).
30. Yoshida, H., Shimada, T. & Ishihama, A. Metal-Responsive Transcription Factors Co-Regulate Anti-Sigma Factor (Rsd) and Ribosome Dimerization Factor Expression. *Int J. Mol. Sci.* **24**, 4717 (2023).
31. Wei, Z. et al. Alternative σ^{I}/anti-σ^{I} factors represent a unique form of bacterial σ/anti-σ complex. *Nucleic Acids Res*. **47**, 5988–5997 (2019).
32. Pardue, E. J. et al. Dual membrane-spanning anti-sigma factors regulate vesiculation in *Bacteroides thetaiotaomicron*. *Proc. Natl Acad. Sci. USA* **121**, e2321910121 (2024).
33. Braetz, S., Schwerk, P., Figueroa-Bossi, N., Tedin, K. & Fulde, M. Prophage Gifsy-1 Induction in *Salmonella enterica* Serovar Typhimurium Reduces Persister Cell Formation after Ciprofloxacin Exposure. *Microbiol Spectr.* **11**, e0187423 (2023).
34. Padalon-Brauch, G. et al. Small RNAs encoded within genetic islands of *Salmonella typhimurium* show host-induced expression and role in virulence. *Nucleic Acids Res*. **36**, 1913–1927 (2008).
35. Venturini, E. et al. A global data-driven census of *Salmonella* small proteins and their potential functions in bacterial virulence. *Microlife* **1**, uqaa002 (2020).
36. Barnhill, E. C. et al. Characterization of novel small RNAs (sRNAs) contributing to the desiccation response of *Salmonella enterica* serovar Typhimurium. *RNA Biol.* **16**, 1643–1657 (2019).
37. Park, J. Y. et al. ChIP-mini: a low-input ChIP-exo protocol for elucidating DNA-binding protein dynamics in intracellular pathogens. *Nucleic Acids Res*. **53**, gkaf009 (2025).
38. Houserova, D. et al. Characterization of 475 Novel, Putative Small RNAs (sRNAs) in Carbon-Starved *Salmonella enterica* Serovar Typhimurium. *Antibiotics* **10**, 305 (2021).
39. Harms, A., Maisonneuve, E. & Gerdes, K. Mechanisms of bacterial persistence during stress and antibiotic exposure. *Science* **354**, aaf4268 (2016).
40. Baran, A., Kwiatkowska, A. & Potocki, L. Antibiotics and Bacterial Resistance-A Short Story of an Endless Arms Race. *Int J. Mol. Sci.* **24**, 5777 (2023).
41. Escalante-Semerena, J. C. & Roth, J. R. Regulation of cobalamin biosynthetic operons in *Salmonella typhimurium*. *J. Bacteriol.* **169**, 2251–2258 (1987).
42. Vance, J. E. Historical perspective: phosphatidylserine and phosphatidylethanolamine from the 1800s to the present. *J. Lipid Res* **59**, 923–944 (2018).
43. Abramson, J. et al. Accurate structure prediction of biomolecular interactions with AlphaFold 3. *Nature* **630**, 493–500 (2024).
44. Lago, M. et al. Proteome remodelling by the stress sigma factor RpoS/σS in *Salmonella*: identification of small proteins and evidence for post-transcriptional regulation. *Sci. Rep.* **7**, 2127 (2017).
45. Maeda, H., Fujita, N. & Ishihama, A. Competition among seven *Escherichia coli* sigma subunits: relative binding affinities to the core RNA polymerase. *Nucleic Acids Res*. **28**, 3497–3503 (2000).
46. Xu, J. et al. Single-Cell and Time-Resolved Profiling of Intracellular *Salmonella* Metabolism in Primary Human Cells. *Anal. Chem.* **91**, 7729–7737 (2019).
47. Kaval, K. G., Garsin, D. A. & Sperandio, V. Ethanolamine utilization in bacteria. *mBio* **9**, e00066–18 (2018).
48. Stingl, K., Altendorf, K. & Bakker, E. P. Acid survival of Helicobacter pylori: how does urease activity trigger cytoplasmic pH homeostasis?. *Trends Microbiol* **10**, 70–74 (2002).
49. Tsoy, O., Ravcheev, D. & Mushegian, A. Comparative genomics of ethanolamine utilization. *J. Bacteriol.* **191**, 7157–7164 (2009).
50. Datsenko, K. A. & Wanner, B. L. One-step inactivation of chromosomal genes in *Escherichia coli* K-12 using PCR products. *Proc. Natl Acad. Sci. USA* **97**, 6640–6645 (2000).
51. Cock, P. J., Fields, C. J., Goto, N., Heuer, M. L. & Rice, P. M. The Sanger FASTQ file format for sequences with quality scores, and the Solexa/Illumina FASTQ variants. *Nucleic Acids Res*. **38**, 1767–1771 (2010).
52. Li, B. & Dewey, C. N. RSEM: accurate transcript quantification from RNA-Seq data with or without a reference genome. *BMC Bioinforma.* **12**, 323 (2011).
53. Mortazavi, A., Williams, B. A., McCue, K., Schaeffer, L. & Wold, B. Mapping and quantifying mammalian transcriptomes by RNA-Seq. *Nat. Methods* **5**, 621–628 (2008).
54. Gaudet, P. & Dessimoz, C. Gene Ontology: Pitfalls, Biases, and Remedies. *Methods Mol. Biol.* **1446**, 189–205 (2017).
55. Kanehisa, M., Sato, Y. & Morishima, K. BlastKOALA and GhostKOALA: KEGG Tools for Functional Characterization of Genome and Metagenome Sequences. *J. Mol. Biol.* **428**, 726–731 (2016).
56. Livak, K. J. & Schmittgen, T. D. Analysis of relative gene expression data using real-time quantitative PCR and the 2(-Delta Delta C(T)) Method. *Methods* **25**, 402–408 (2001).
57. Li, B. et al. *Salmonella* STM1697 coordinates flagella biogenesis and virulence by restricting flagellar master protein $FlhD_4C_2$ from recruiting RNA polymerase. *Nucleic Acids Res*. **45**, 9976–9989 (2017).
58. Otwinowski, Z. & Minor, W. Processing of X-ray diffraction data collected in oscillation mode. *Methods Enzymol.* **276**, 307–326 (1997).
59. Adams, P. D. et al. PHENIX: building new software for automated crystallographic structure determination. *Acta Crystallogr D. Biol. Crystallogr* **58**, 1948–1954 (2002).
60. Emsley, P. & Cowtan, K. Coot: model-building tools for molecular graphics. *Acta Crystallogr D. Biol. Crystallogr* **60**, 2126–2132 (2004).
61. Chen, T. et al. The Genome Sequence Archive Family: Toward Explosive Data Growth and Diverse Data Types. *Genomics Proteom. Bioinforma.* **19**, 578–583 (2021).
62. CNCB-NGDC Members and Partners Database Resources of the National Genomics Data Center, China National Center for Bioinformation in 2024. *Nucleic Acids Res*. **52**, D18–D32 (2024).

Acknowledgements

This work was supported by the National Natural Science Foundation of China [32170034 and 81902038], the Taishan Scholar Project of Shandong

Province [tsqn202211216], the Natural Science Foundation of Shandong Province [ZR2023YQ060, ZR2024MC045 and ZR2024QC209], the Youth Innovation Technology Program innovation team of Shandong Provincial University [2023KJ170], Medicine and Health Science Technology Development Plan of Shandong Province [202201060464], the Joint Innovation Team for Clinical & Basic Research of Shandong First Medical University [202410], Key Project in Medical and Health Technology of Shandong Province [202401060550].

Author contributions

B.L. and W.W. contributed to the conception and design of the study. R.L. and B.L. conceived and drafted the manuscript. R.L. performed the phenotypic assays, transcriptomics analysis, protein structure and evolutionary analysis. Q.W. and X.Y. performed crystal structure assays and protein interaction test. Y.Y., P.Z., and K.Y. performed data analysis. All authors have contributed to the manuscript and approved the submitted version.

Competing interests

The authors declare no competing interests.

Additional information

Supplementary information The online version contains supplementary material available at https://doi.org/10.1038/s42003-025-08989-7.

Correspondence and requests for materials should be addressed to Weiwei Wang or Bingqing Li.

Peer review information *Communications Biology* thanks Glen M. Borchert and the other, anonymous, reviewers for their contribution to the peer review of this work. Primary Handling Editors: Laura Rodríguez Pérez. A peer review file is available.

Reprints and permissions information is available at http://www.nature.com/reprints

Publisher's note Springer Nature remains neutral with regard to jurisdictional claims in published maps and institutional affiliations.

Open Access This article is licensed under a Creative Commons Attribution-NonCommercial-NoDerivatives 4.0 International License, which permits any non-commercial use, sharing, distribution and reproduction in any medium or format, as long as you give appropriate credit to the original author(s) and the source, provide a link to the Creative Commons licence, and indicate if you modified the licensed material. You do not have permission under this licence to share adapted material derived from this article or parts of it. The images or other third party material in this article are included in the article's Creative Commons licence, unless indicated otherwise in a credit line to the material. If material is not included in the article's Creative Commons licence and your intended use is not permitted by statutory regulation or exceeds the permitted use, you will need to obtain permission directly from the copyright holder. To view a copy of this licence, visit http://creativecommons.org/licenses/by-nc-nd/4.0/.

© The Author(s) 2025